

A Lipid Pathway for Ligand Binding Is Necessary for a Cannabinoid G Protein-coupled Receptor^{*§}

Received for publication, July 6, 2009, and in revised form, February 13, 2010. Published, JBC Papers in Press, March 10, 2010, DOI 10.1074/jbc.M109.041590

Dow P. Hurst[†], Alan Grossfield[§], Diane L. Lynch[‡], Scott Feller[¶], Tod D. Romo[§], Klaus Gawrisch^{||}, Michael C. Pitman^{**}, and Patricia H. Reggio[†]

From the [†]Department of Chemistry and Biochemistry, Center for Drug Discovery, University of North Carolina, Greensboro, North Carolina 27402, the [§]Department of Biochemistry and Biophysics, University of Rochester Medical Center, Rochester, New York 14642, the [¶]Department of Chemistry, Wabash College, Crawfordsville, Indiana 47933, ^{||}Membrane Biochemistry/Biophysics, NIAAA, National Institutes of Health, Bethesda, Maryland 20892, and the ^{**}Computational Biology Center, IBM Thomas J. Watson Research Center, Yorktown Heights, New York 10598

Recent isothiocyanate covalent labeling studies have suggested that a classical cannabinoid, (−)-7'-isothiocyanato-11-hydroxy-1',1'dimethylheptyl-hexahydrocannabinol (AM841), enters the cannabinoid CB2 receptor via the lipid bilayer (Pei, Y., Mercier, R. W., Anday, J. K., Thakur, G. A., Zvonok, A. M., Hurst, D., Reggio, P. H., Janero, D. R., and Makriyannis, A. (2008) *Chem. Biol.* 15, 1207–1219). However, the sequence of steps involved in such a lipid pathway entry has not yet been elucidated. Here, we test the hypothesis that the endogenous cannabinoid *sn*-2-arachidonoylglycerol (2-AG) attains access to the CB2 receptor via the lipid bilayer. To this end, we have employed microsecond time scale all-atom molecular dynamics (MD) simulations of the interaction of 2-AG with CB2 via a palmitoyl-oleoyl-phosphatidylcholine lipid bilayer. Results suggest the following: 1) 2-AG first partitions out of bulk lipid at the transmembrane α -helix (TMH) 6/7 interface; 2) 2-AG then enters the CB2 receptor binding pocket by passing between TMH6 and TMH7; 3) the entrance of the 2-AG headgroup into the CB2 binding pocket is sufficient to trigger breaking of the intracellular TMH3/6 ionic lock and the movement of the TMH6 intracellular end away from TMH3; and 4) subsequent to protonation at D3.49/D6.30, further 2-AG entry into the ligand binding pocket results in both a W6.48 toggle switch change and a large influx of water. To our knowledge, this is the first demonstration via unbiased molecular dynamics that a ligand can access the binding pocket of a class A G protein-coupled receptor via the lipid bilayer and the first demonstration via molecular dynamics of G protein-coupled receptor activation triggered by a ligand binding event.

The cannabinoid receptors belong to the class A (rhodopsin family) of G protein-coupled receptors (GPCRs).² The

second cannabinoid receptor subtype, CB2 (2), is highly expressed throughout the immune system (3, 4) and has been described in the central nervous system under both pathological (5) and physiological conditions (6). All known CB2 ligands are highly lipophilic. In fact, the CB2 endogenous cannabinoid, *sn*-2-arachidonoylglycerol (2-AG) (7, 8), is synthesized on demand from the lipid bilayer itself in a two-step process in which phospholipase C- β hydrolyzes phosphatidylinositol 4,5-bisphosphate to generate diacylglycerol, which is then hydrolyzed by diacylglycerol lipase to yield 2-AG (9, 10). After 2-AG interaction with the membrane-embedded CB receptor, it is hydrolyzed to arachidonic acid and glycerol by a membrane-associated enzyme, monoacylglycerol lipase (11).

As revealed by the crystal structures of rhodopsin (12–15), the β_2 -adrenergic receptor (AR) (16–18), β_1 -AR (19), and adenosine A2A receptor (20), the general topology of a GPCR includes the following: 1) an extracellular (EC) N terminus; 2) seven transmembrane α -helices (TMHs) arranged to form a closed bundle; 3) loops connecting TMHs that extend intra- and extracellularly; and 4) an intracellular (IC) C terminus that begins with a short helical segment (helix 8) oriented parallel to the membrane surface. Agonists bind inside the crevice formed by the TMH bundle and produce conformational changes on the IC face of the receptor that uncover previously masked G protein-binding sites (21), which then lead to G protein coupling. Biophysical studies using a variety of techniques indicate that ligand-induced receptor activation produces the following changes: 1) a conformational change in the W6.48 “toggle switch” within the ligand binding pocket (22); 2) a change in the relative orientations of TMH3 and -6 that breaks an IC “ionic lock” (23–28), with the intracellular end of TMH6 moving away from TMH3 by hinging and moving up toward lipid (27); 3) the uptake of two protons (29); and 4) an influx of water (30).

Recent isothiocyanate covalent labeling studies have suggested that a classical cannabinoid, AM841, enters the CB2 receptor via the lipid bilayer (1). However, the sequence of steps involved in such a lipid pathway entry has not yet been elucidated. We report here microsecond time scale unbiased

* This work was supported, in whole or in part, by National Institutes of Health Grants DA003934 and DA021358 (to P. H. R.) from NIDA and by grants from NIAAA, Intramural Research program (to K. G.). This work was also supported by National Science Foundation Grant MCB-0543124 (to S. F.).

§ The on-line version of this article (available at <http://www.jbc.org>) contains supplemental Table S1.

[¶] To whom correspondence should be addressed: Dept. of Chemistry and Biochemistry, University of North Carolina, P. O. Box 26170, Greensboro, NC 27412. Tel.: 336-334-5333; Fax: 336-334-5402; E-mail: phreggio@uncg.edu.

² The abbreviations used are: GPCR, G protein-coupled receptor; 2-AG, *sn*-2-arachidonoylglycerol; MD, molecular dynamics; AR, adrenergic receptor;

EC, extracellular; IC, intracellular; TMH, transmembrane α -helix; SASA, solvent-accessible surface area.



MD simulations of the interaction of 2-AG with the CB2 receptor via the lipid bilayer. We show that 2-AG first partitions out of bulk lipid at the TMH6/7 interface and then enters the CB2 receptor binding pocket via a portal that forms between TMH6 and TMH7. Furthermore, our simulations reveal that the entry of 2-AG into CB2 produces conformational changes in the intracellular domains of CB2 that are commonly associated with GPCR activation (31).

MATERIALS AND METHODS

Amino Acid Numbering System—The Ballesteros and Weinstein (32) amino acid numbering system used here begins with the TMH number, followed by a locant (.50 assigned to most highly conserved amino acid in a TMH and other residues numbered relative to it), and the absolute sequence number in parentheses. Loop residues are designated by their absolute sequence numbers in parentheses only.

Model of Inactive State (R) Form of CB2—The CB2 inactive state (R) model used here includes the TMHs, EC and IC loops, and the N and C termini, with a putative palmitoylation site at C(320). Although this model used a rhodopsin template (12), it has undergone extensive refinements to better reflect sequence-dictated differences between CB2 and rhodopsin. A discussion of these differences as well as model construction details are provided in our recent paper (33). The resulting model has been tested via mutation (34), substituted cysteine accessibility (33, 35), and isothiocyanate labeling studies (1).

Molecular Dynamics Simulations—Fig. 1 outlines the sequence of MD runs reported here.

Inactive Receptor—For preliminary calculations, the CB2 model was embedded in a bilayer containing 99 stearoyl-docosahexaenyl-phosphatidylcholine (SDPC) lipid molecules; the membrane was generated *de novo* using a library of lipid conformations from previous neat lipid simulations, as described in Grossfield *et al.* (36). The system was warmed over the course of 1 ns, using velocity resampling every 5 ps, and then run in the NVT ensemble for ~300 ns at 310 K with the box size fixed at 54 × 76.2 × 95.5 Å. The system was equilibrated for 20 ns before a 286-ns production run was initiated.

After the 286-ns trajectory of CB2 in lipid (trajectory A, described above) was complete, production simulations were initiated that contained the complete CB2 model, using the final protein conformation from trajectory A, embedded in a bilayer containing 123 palmitoyl-oleoyl-phosphatidylcholine lipid molecules and 38 2-AG molecules. The bilayer system was solvated by 9965 water molecules, 14 sodium ions, and 31 chloride ions to yield an electrically neutral system with roughly 100 mM salt. The CHARMM27 force field for proteins and lipids was used (37–39). Repulsion-dispersion interactions were smoothly truncated at 10 Å, and the particle-particle-particle-mesh Ewald method was used to compute long range electrostatics, using a 128³ grid for the fast Fourier transform, a charge interpolation distance of four mesh points, and the Ewald α value set to 0.35 Å⁻¹. The temperature was held at 310 K using velocity resampling every 1 ns, and the system volume was held fixed at 74.1 × 74.1 × 96.7 Å. The dynamics were integrated using the velocity Verlet integrator (40), with a time step of 2 fs and

bonds to hydrogen constrained using RATTLE with the tolerance set to 10⁻¹⁰ (41). Previous work has shown that this protocol leads to excellent energy conservation, with temperature drifts of roughly 1 K over a microsecond of dynamics (30). Production dynamics was performed on the Blue Gene/W supercomputer (42, 43) located at the T. J. Watson Research Center, typically on 4096 dual-core nodes, using Blue Matter, a simulation package developed at IBM specifically to take advantage of the Blue Gene architecture (43, 44).

Production dynamics was performed at constant volume, using either NVT (performed using velocity resampling every 1 ns) or NVE. This follows our protocol previously applied to rhodopsin (30, 36, 45–47). In developing the protocol, we have specifically investigated the consequences of long time constant volume simulations for membrane-GPCR systems, after the volume has been equilibrated to 1 atm of pressure. We found, and it has been reviewed in the citations above, that with an initial equilibration of the system volume under normal pressure, the volume may be fixed for the production period of the simulation. This was monitored by the order parameters of the lipid chains, which respond to changes in pressure by expansion or contraction, which is reflected by changes in lipid order. Lipid order parameters remain stable after system equilibration, and therefore NVT or NVE is not problematic in the present case.

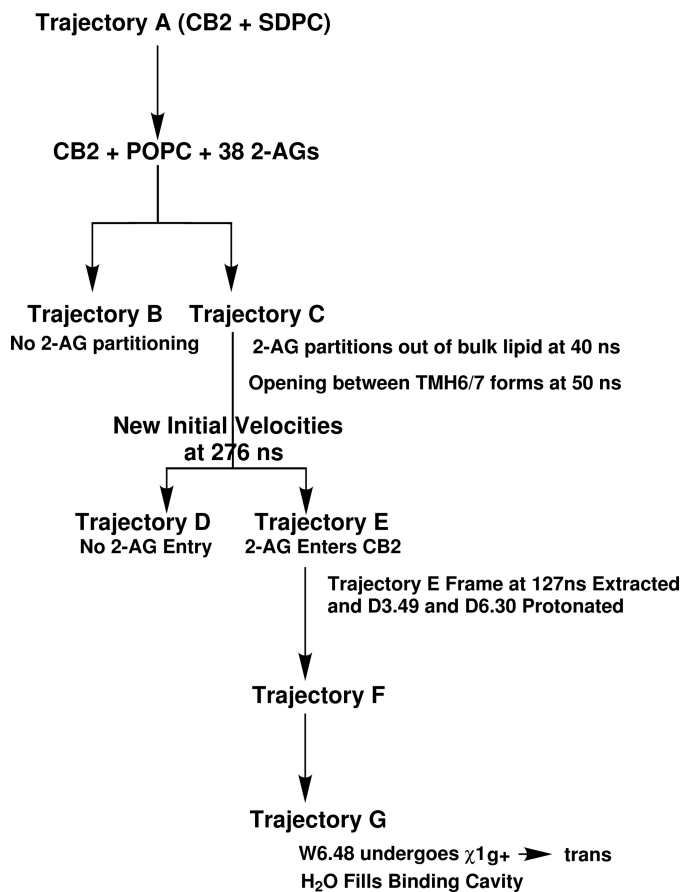
After warm-up and equilibration, two separate simulations (trajectory B and C) were constructed using identical protein structures and regenerating the lipid and 2-AG conformations using different random number seeds (36). Trajectory B showed no 2-AG partitioning out of bulk lipid. In contrast, in trajectory C (at 276 ns), one 2-AG molecule partitioned out of bulk lipid and associated with the TMH6/TMH7 CB2 lipid face. This frame was used as the starting point for two separate simulations (trajectories D and E) begun by randomly selecting new initial velocities from the Maxwell-Boltzmann distribution at physiological temperature (37 °C). In trajectory E, 2-AG entered CB2. In trajectory D, 2-AG did not enter CB2; therefore, trajectory D is used here as a control.

To generate a protonated form of activated CB2, the trajectory E frame at 127 ns was extracted, and both D3.49(130) and D6.30(240) were protonated with a corresponding removal of two sodium ions from bulk to preserve system neutrality. The initial protonated structure was equilibrated (NVT) first with velocity resampling at 310 K with a resampling interval of 200 fs for a duration of a few hundred ps (365 ps), followed by a resampling interval of 1 ps for a few nanoseconds (5.488 ns). Equilibration was followed by production with a 1-ns resampling for nearly 2 μs (1954 ns) NVT. NVE conditions were then applied to the end of trajectory F, giving trajectory G (no further velocity resampling). Trajectory G production resumed for nearly 1.7 μs (1668 ns) under NVE conditions with excellent energy conservation. Consistent with previous NVE production simulations with the present conditions, the temperature increased <1 K over the 1.7 μs of NVE for trajectory G.

R3.55-D6.30 Salt Bridge Calculations—Musafia *et al.* (48) have reported that the average interatomic N-O distance for a

Lipid Pathway for CB2 Ligand Binding

Simulation Flowchart



simple Arg-Asp salt bridge is 2.93 Å. All measurements of salt bridge distances were made using Visual Molecular Dynamics (49). Trajectory frames for which the N(R3.55)-O(D6.30) distance was 4 Å or greater were considered to lack salt bridge interactions.

SASA Calculations—Solvent-accessible surface area calculations were performed with the built in measure commands available in Visual Molecular Dynamics (49). A 1.4-Å probe radius was used.

2-AG Pathway Calculations—The percent contact data for 2-AG entering CB2 was obtained as follows: a residue was counted in contact with 2-AG if any of its heavy atoms were within 4.0 Å of the specified 2-AG atoms. This contact was recorded for each frame in the trajectory, from which a percentage was calculated. Hydrogen bonds were calculated using a 3.5-Å cutoff for heavy atom distance and a D-H...A angle limit of 120° (*i.e.* D-H...A angle >120°).

Water Density—The water “density” visualizations in Fig. 11 were constructed by first aligning each frame of the trajectory such that the CB2 transmembrane α-carbons were superimposed upon an average structure. A 1-Å resolution density grid was then superimposed over the system. At each time point (trajectory frame), internal waters were picked out by only considering water oxygen atoms that were within a 30-Å radius of the principal axis formed from all CB2 α-carbons. There was no

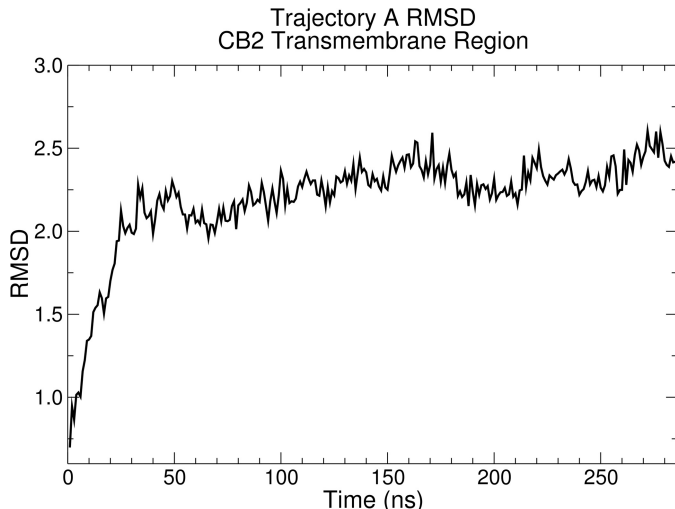


FIGURE 2. This plot of root mean square deviation (RMSD) versus time for trajectory A (see Fig. 1) shows that the CB2 inactive state model stabilized within the first 50 ns.

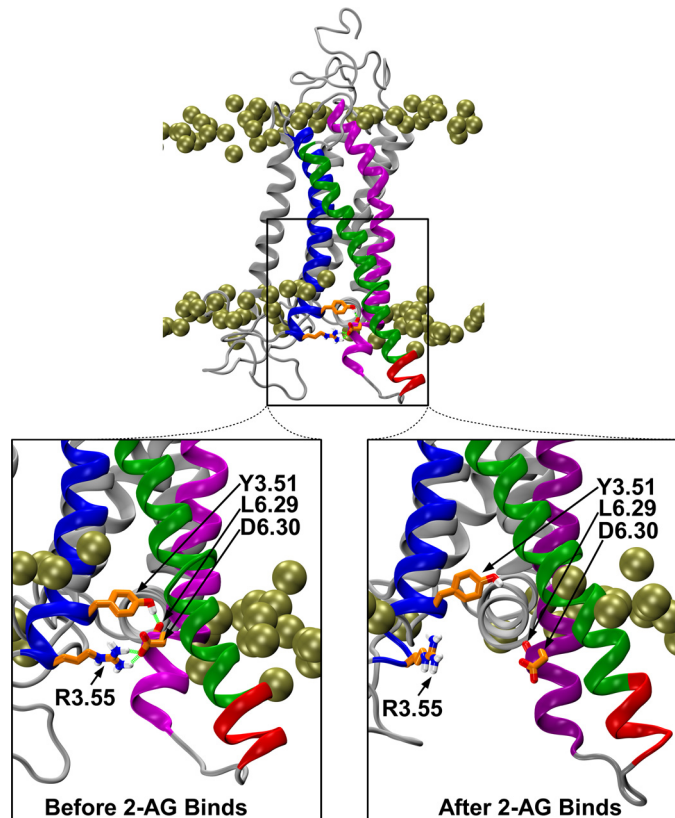
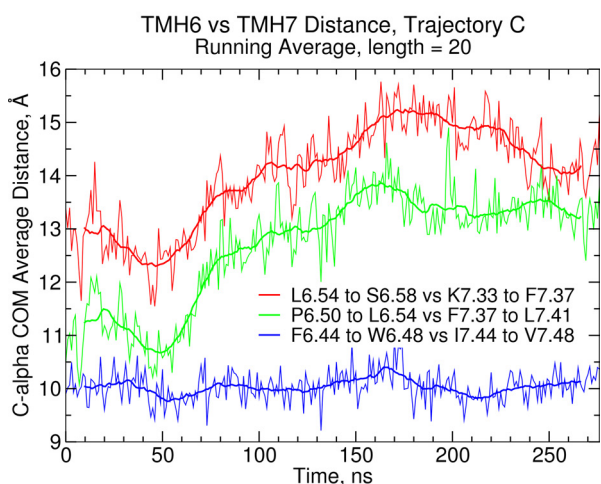
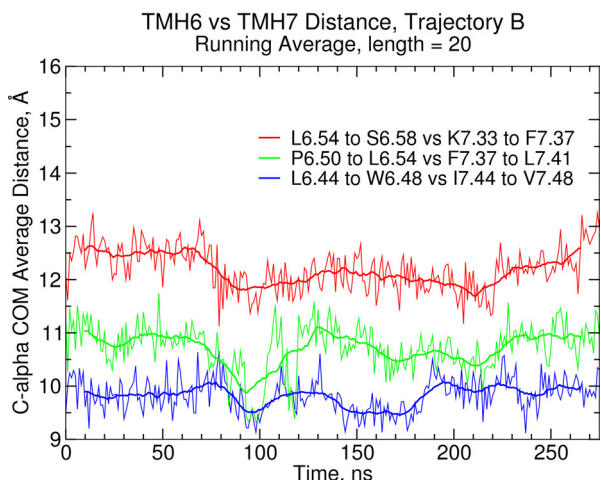
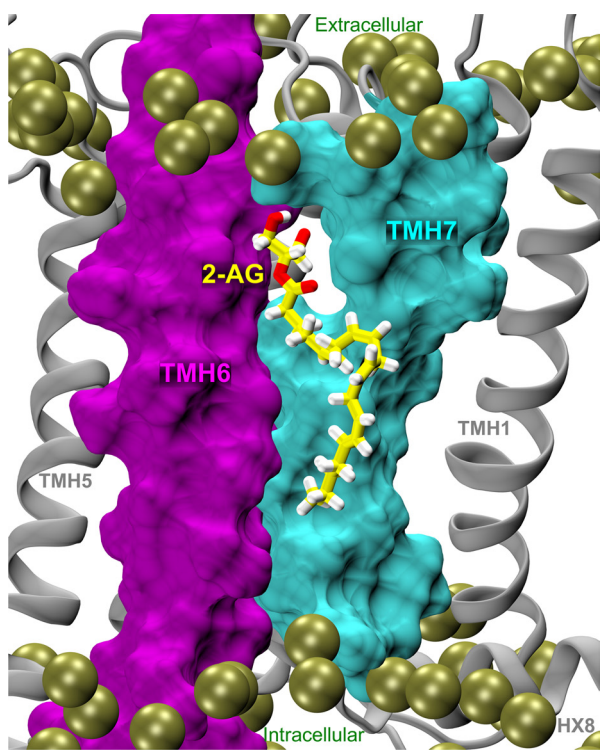


FIGURE 3. Relationship between the intracellular ends of TMH3 and TMH6 at designated points along the simulation is illustrated here. The CB2 TMH bundle is shown in ribbon format with phosphorus atoms of the bilayer highlighted in gold. TMHs shown in color include TMH3 (blue), TMH5 (green with red intracellular extension), and TMH6 (magenta). Top and lower left, although we began trajectory A with a salt bridge between R3.50(131) and D6.30(240) at the IC ends of TMH3/6, the receptor rearranged to form a salt bridge between R3.55(136) and D6.30(240), with Y3.51(132) hydrogen bonding to the exposed backbone carbonyl of L6.29(239). In addition, the IC-3 loop assumed two additional helical turns (shown here in red). Lower right, this figure shows the broken R3.55(136)/D6.30(240) salt bridge and the broken Y3.51(132)/L6.29(239) carbonyl interaction at 184 ns into trajectory E (compare with lower left).

Lipid Pathway for CB2 Ligand Binding



height cutoff imposed along the principal axis, so a “cap” of bulk waters are included to help visualize the bulk water interface. A 2-Å sphere of density was then superimposed about the coordinates of each water oxygen that was then averaged into the grid. The resulting density map was then scaled so all density values ranged from 0 to 1. All analyses were performed using the “Lightweight Object Oriented Structure Analysis” package (or “LOOS”) (50) and available via SourceForge and custom software.

RESULTS

Molecular Dynamics Simulations—The sequence of trajectories reported here is summarized in Fig. 1. Fig. 2 shows that the root mean square deviation of the CB2 inactive state model stabilized within the first 50 ns of trajectory A. Certain interactions in the CB2 inactive state model input for the MD runs remained stable, such as the salt bridge between K3.28(109) and D(275) in the CB2 EC-3 loop. Other interactions that have important implications for both ligand recognition and activation of CB2 changed early in the simulation. First, although the simulation was begun with an aromatic stacking interaction between F3.36(117) and W6.48(258) (analogous to the CB1 toggle switch (51)), F3.36(117) shifted toward TMH5 during the equilibration, and W6.48(258) established a hydrogen bond with N7.45(291). Second, although the simulation was begun with a salt bridge between R3.50(131) and D6.30(240) at the intracellular ends of TMH3/6 analogous to the R3.50/E6.30 salt bridge in the dark state of rhodopsin (12), the receptor rearranged quickly to form a salt bridge between R3.55(136) and D6.30(240), with Y3.51(132) hydrogen bonding to the exposed backbone carbonyl of L6.29(239). This produces a network that reinforces the interaction between the IC ends of TMH3 and TMH6 (Fig. 3). Third, the IC-3 loop assumed additional structure by the addition of at least two helical turns to the original end of TMH5 (Fig. 3 in red).

Ligand Entry into CB2 and Subsequent Changes in Intracellular Domains—The final protein conformation at the end of trajectory A (286 ns) was used as input to new simulations. Thirty eight 2-AG and 123 palmitoyl-oleoyl-phosphatidylcholine molecules were distributed randomly around the CB2 receptor bundle (36). After warm-up and equilibration, two separate simulations (trajectory B and C) were constructed using identical protein structures and regenerating the lipid and 2-AG conformations using a different random number of seeds (see Fig. 1) (36). Trajectory B showed no 2-AG partitioning out of bulk lipid and is used as a control here. In contrast, in trajectory C (at 40 ns), a 2-AG molecule partitioned out of bulk lipid and established a long lasting direct interaction with the CB2 TMH6/TMH7 lipid face.

FIGURE 4. Top, at 13 ns into trajectory E, 2-AG (yellow) is poised to enter CB2 between TMH6 (magenta) and TMH7 (cyan) (shown in surface view) via an opening above W6.48(258) at the level of the β_{10} helical region of TMH7, which formed in trajectory C. Middle, in the control trajectory (trajectory B) for which no 2-AG partitioning out of bulk lipid occurred, the distances between the centers of mass on TMH6 and TMH7 at three different levels show no major changes. Bottom, in contrast in trajectory C, an increase in distance between TMH6/7 occurs only extracellular to W6.48.

Lipid Pathway for CB2 Ligand Binding

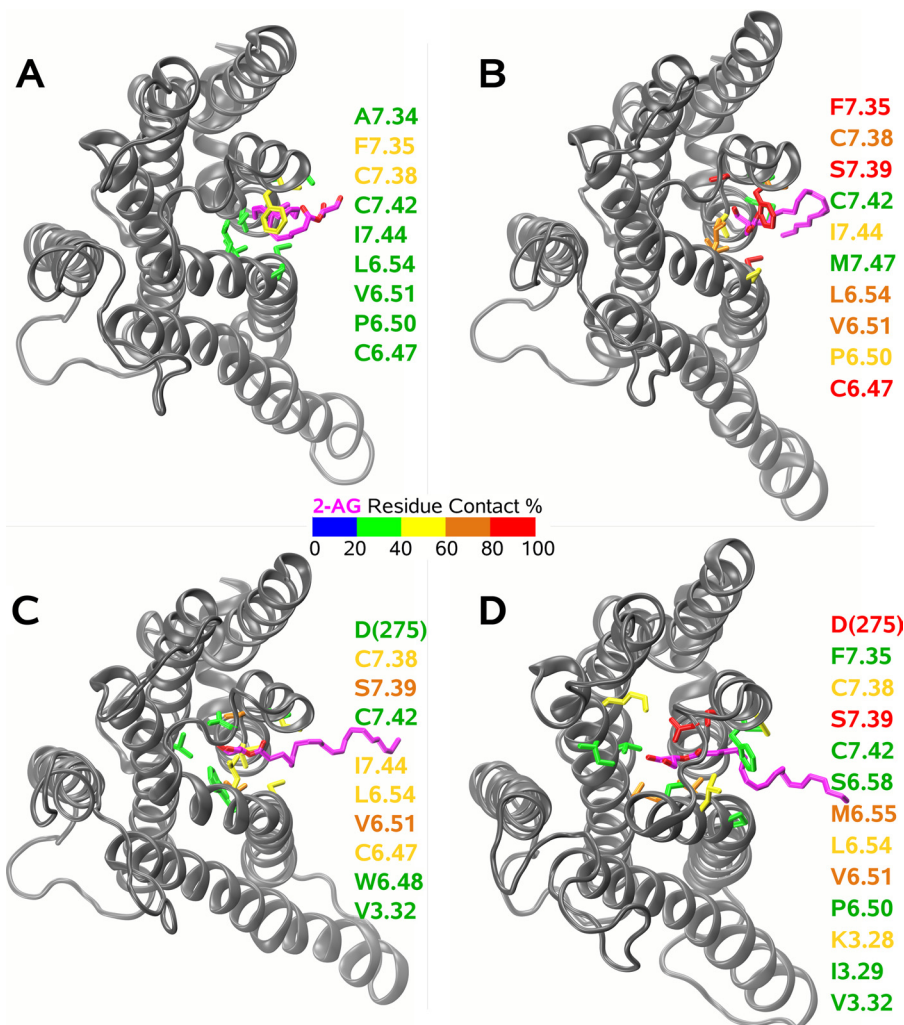


FIGURE 5. This figure illustrates the progress of 2-AG into the binding pocket. The color scale represents the percentage of the trajectory in which any portion of 2-AG is within 4 Å of residues on CB2 (defined here as within contact distance). Residues within contact distance are listed on the right and are color-coded according to this scale. *A*, in trajectory C (40–275 ns), the 2-AG has partitioned out of bulk lipid and contacts residues in or near the TMH6/7 interface. Highest contact is with F7.35(281) and C7.38(284). *B*, in trajectory E (0–52 ns; up to the point of headgroup insertion), 2-AG interaction with residues in the TMH6/7 interface increases with greater than 80% contact occurring with F7.35(281), S7.39(285), and C6.47(257). *C*, in trajectory E, after 2-AG entry into CB2 (53–127 ns), 2-AG begins to contact binding pocket residues on TMH3 (V3.32(113)), TMH6 (W6.48(258)), TMH7 (C7.42(288)), and the EC-3 loop (D(275)). *D*, subsequent to protonation, in trajectory G (from 913 to 1668 ns), 2-AG contacts multiple residues on TMH3/6/7 and the EC-3 loop with formation of hydrogen bonds with D(275) in the EC-3 loop and to a lesser extent with S7.39(285) (see supplemental Table S1).

Subsequent to this partitioning, at 50 ns (trajectory C), an opening formed between TMH6/TMH7 above W6.48 and in the 3₁₀-helical region of TMH7 (C7.42-M7.47) (Fig. 4, *top*). Fig. 4, *bottom*, shows that this increase in distance between TMH6/7 occurs extracellular to W6.48 in trajectory C, and Fig. 4, *middle*, shows no corresponding change in TMH6/7 distance in trajectory B.

No 2-AG entry into CB2 occurred in trajectory C. As a result, a frame from trajectory C (at 276 ns) was used as the starting point for two separate simulations (trajectories D and E) that were begun by randomly selecting new initial velocities from a Maxwell-Boltzmann distribution at physiological temperature (37 °C). In trajectory D, no 2-AG entry occurred, so this trajectory is used here as a control. In trajectory E, the partitioned 2-AG entered CB2 by passing between TMH6/TMH7. This

simulation exhibits many of the elements associated with GPCR activation, as will be discussed below.

Ligand Entry—Fig. 5 illustrates the progress of 2-AG into the binding pocket at four different time periods during the simulations, and supplemental Table S1 details the 2-AG hydrogen bonding patterns that occur for the same time periods. In trajectory C (Fig. 5*A*; 40–275 ns), the 2-AG partitioned out of bulk lipid and spends the highest percentage time within 4 Å of residues in or near the TMH6/7 interface, particularly, F7.35(281) and C7.38(284). The headgroup hydroxyls of 2-AG are engaged in hydrogen bonds predominantly with water and also with each other (*i.e.* intramolecular hydrogen bonding). In trajectory E (0–52 ns; Fig. 5*B*) up to the point of headgroup insertion, 2-AG interaction with residues in the TMH6/7 interface increases with 2-AG in greater than 80% of the trajectory interval within 4 Å of F7.35(281), S7.39(285), and C6.47(257). Intramolecular hydrogen bonding and hydrogen bonding with water remain predominant interactions for the headgroup hydroxyls, although the ester oxygens form few hydrogen bonds. At 54 ns into trajectory E, the headgroup of 2-AG inserts into the CB2-binding site crevice. In trajectory E after 2-AG entry into CB2 (54–127 ns; Fig. 5*C*), 2-AG is in close proximity to binding pocket residues on TMH3 (V3.32(113)), TMH6 (W6.48(258)), TMH7 (C7.42(288)), and the EC-3 loop (D(275)). Hydrogen bonding to water and intramolecular hydrogen bonding remains a predominant interaction for the headgroup hydroxyls, with some hydrogen bonding to D(275) and S6.58(268) occurring. The ester oxygens form few hydrogen bonds. A discussion of Fig. 5*D* is given below for the protonated trajectories.

Changes in Intracellular Domains—Five ns after ligand entry, at 59 ns into trajectory E, both the D6.30(240)/R3.55(136) salt bridge and the Y3.51(132)/L6.29(239) hydrogen bond break (Fig. 3, *lower right*). The IC helical extensions of TMH5 and TMH6 (IC-3 loop) then hinge and move away from the TMH bundle and up into lipid. Fig. 6*a* shows the receptor before 2-AG entry at 1 ns into trajectory E. Fig. 6*b* shows the receptor after 2-AG entry at 184 ns into trajectory E, which is 130 ns after 2-AG entry. Fig. 6*c* was taken from trajectory E saved at 10-ps

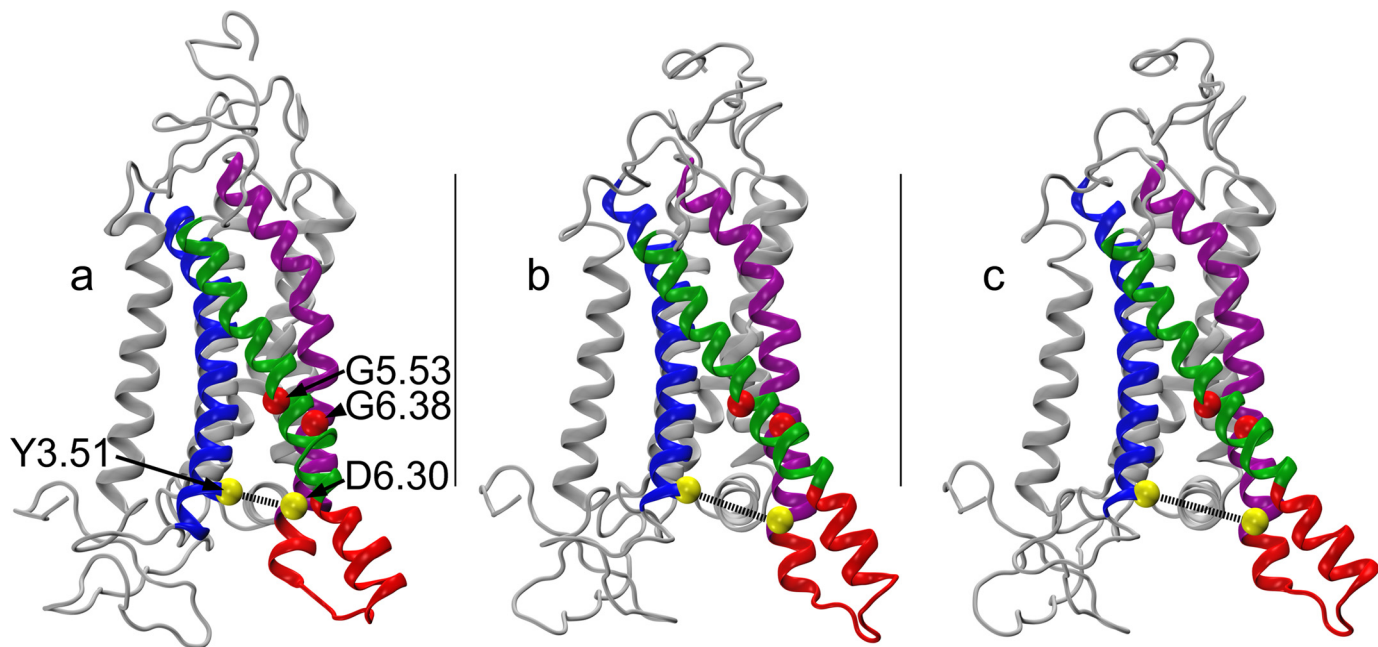


FIGURE 6. Effect of 2-AG entry into CB2 is illustrated here. The CB2 TMH bundle is shown in ribbon format. TMHs shown in color include TMH3 (blue), TMH5 (green), and TMH6 (magenta). The IC-3 loop is shown in red. *a*, receptor before 2-AG entry at 1 ns into trajectory E; *b*, 130 ns after 2-AG entry; and *c*, 131.14 ns after 2-AG entry. The C- α distances between Y3.51(132) and D6.30(240) (yellow balls) are 7.56 Å (*a*), 12.05 Å (*b*), and 13.86 Å (*c*). The hinge points for the movement of the IC helical extensions of TMH5 and TMH6 are G5.53(204) and G6.38(248) (shown in red in Fig. 6). The opening created at 185.14 ns into trajectory E (Fig. 6*C*) approaches the size of the opening on the IC side of the bovine opsin*-G α C-terminal peptide complex which is 14.5 Å (52).

intervals. This shows that the widest opening at the intracellular ends of TMH3/6 occurs at 185.14 ns into trajectory E. This is 131.14 ns after 2-AG entry. The Y3.51(132) to D6.30(240) C- α distances are as follows: (*a*) 7.56 Å, (*b*) 12.05 Å, and (*c*) 13.86 Å. The hinge points for the movement of the IC helical extensions of TMH5 and TMH6 are G5.53(204) and G6.38(248) (shown in red in Fig. 6). The opening created at 185.14 ns into trajectory E (Fig. 6*C*) approaches the size of the opening on the IC side of the bovine opsin*-G α C-terminal peptide complex which is 14.5 Å (52).

Fig. 7 (*top*) shows that the widening between TMH3/6 is not due to a general separation of the helices as the distance between residues away from the TMH3/6 IC ends do not change substantially over the trajectory (e.g. V3.40(121) to A6.42(252) distance (*red*) or L3.44(125) to G6.38(248) distance (*green*)), but the distance between residues near the TMH3/6 IC ends (*i.e.* A3.47(128) to A6.34(244) distance (*blue*) and Y3.51(132) to D6.30(240) distance (*black*)) shows a significant widening from time point 59 ns into trajectory E, which is 5 ns after 2-AG enters CB2 (*a purple arrowhead* marks this entry time point). In contrast, Fig. 7 (*bottom*) shows that in the control trajectory (trajectory D), there are no significant changes in the TMH3/6 distance.

Ionic Lock—As mentioned above, during the equilibration phase, the CB2 receptor model rearranged to form a salt bridge between R3.55(136) and D6.30(240), with Y3.51(132) hydrogen bonding to the exposed backbone carbonyl of L6.29(239). This ionic lock was broken 5 ns after ligand entry, at 59 ns into trajectory E (Fig. 3, *lower right*). R3.55(136) is intracellular to the arginine typically involved in the ionic lock, R3.50(131). R3.50(131) has been shown to be protected from the cytoplasm in the inactive state of the GnRH receptor by an “arginine cage” that includes the hydrophobic res-

idue I3.54 that shields R3.50 from water and thereby strengthens the ionic lock salt bridge (53). Fig. 8 illustrates a comparison of the SASAs of CB2 residues R3.50(131), R3.55(136), and R(229), the latter being a CB2 IC-3 loop residue. In Fig. 8 (*top*), the SASAs of these three arginines are shown for trajectory C + D in which no ligand binding event occurred. It is clear here that the SASAs of R3.50(131) and R3.55(136) are comparable when no ligand entry occurs and that, consistent with its location on the IC3 loop, the SASA for R(229) is higher than that of R3.50(131) or R3.55(136). In Fig. 8 (*bottom*), these SASAs are shown for trajectory C + E in which ligand entry occurred at 54 ns into trajectory E (marked by *purple arrowhead*). It is clear here that the SASAs of R3.50(131) and R3.55(136) are comparable before ligand entry, and after ligand entry in trajectory E, the R3.55(136) SASA increases due to the intracellular movement of TMH6 away from TMH3 and resultant increased exposure of R3.55(136) to solvent.

Protonated Receptor Trajectory—As illustrated in Fig. 7 (*top*), 133 ns after the intracellular end of CB2 opened (with 2-AG entry), the salt bridge between D6.30(240) and R3.55(136) re-formed and the IC-3 loop hinged back to its original position. It has been shown for rhodopsin that subsequent to the movement of TMH6, an uptake of two protons occurs (54). We reasoned that the R3.55(136)/D6.30(240) salt bridge restoration was because this protonation step had not occurred. Therefore, a frame (in which the salt bridge is broken) was extracted from trajectory E (at 127 ns; indicated by the *orange arrowhead* in Fig. 7(*top*)). Both D3.49(130) and D6.30(240) were then protonated, and a new trajectory, trajectory F, was initiated. Equilibration was followed by production with velocity resampling every 1 ns for nearly 2 μ s (1954 ns) NVT. NVE conditions were then applied to the end of trajec-

Lipid Pathway for CB2 Ligand Binding

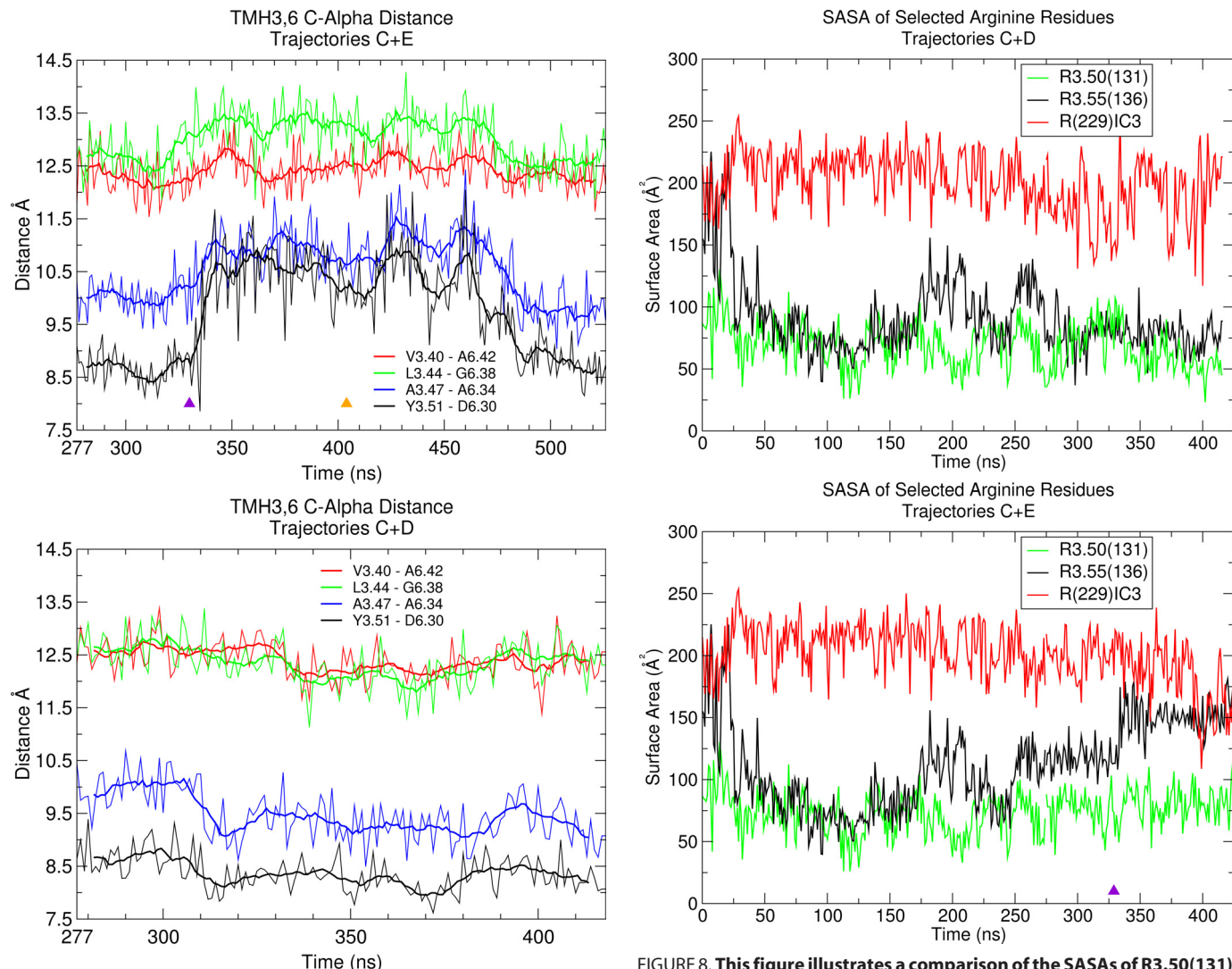


FIGURE 7. Top, change in the distance between TMH3/6 in trajectory E is illustrated that occurs near the IC side of the receptor (A3.47(128) to A6.34(244) distance (blue) and Y3.51(132) to D6.30(240) distance (black)) starting at 59 ns into trajectory E, which is 5 ns after 2-AG enters CB2 (ligand entry time point marked by purple arrowhead). The distance between residues more EC do not change substantially (V3.40(121) to A6.42(252) distance (red) or L3.44(125) to G6.38(248) distance (green)). In contrast, bottom shows that in the control trajectory (trajectory D), there are no significant changes in the distance between TMH3/6. The orange arrowhead in top marks the time point frame used for protonation studies.

jectory F, giving trajectory G (no further velocity resampling). Trajectory G production resumed for 1.668 μ s under NVE conditions. Fig. 9 is a plot of the N(R3.55(136))-O(D6.30(240)) distance *versus* time for the sequence: trajectory C \rightarrow E (up to protonation point) \rightarrow trajectory F \rightarrow G. The purple arrowhead in Fig. 9 marks the point of 2-AG entry, and the orange arrowhead marks the point at which CB2 was protonated. Here trajectory frames for which the N(R3.55(136))-O(D6.30(240)) distance was 4 Å or greater were considered to lack salt bridge interactions (48). As illustrated in Fig. 9 at the orange arrowhead and beyond, the salt bridge between R3.55(136) and D6.30(240) remained broken (except for some random fluctuations) throughout both trajectory F and G.

2-AG/CB2 Interactions in Protonated Receptor Trajectories—Fig. 5D illustrates the position and contacts for 2-AG in tra-

FIGURE 8. This figure illustrates a comparison of the SASAs of R3.50(131), R3.55(136), and R(229), the latter being a CB2 IC-3 loop residue. Top, SASAs of these three arginines are shown for trajectory C + D in which no ligand binding event occurred. Bottom, these SASAs are shown for trajectory C + E in which ligand entry occurred at 54 ns into trajectory E (marked by purple arrowhead).

jectory G (from 913 to 1668 ns), and supplemental Table S1 details the hydrogen bonding patterns that occur for this time period. Subsequent to protonation, in trajectory G (from 913 to 1668 ns), 2-AG contacts multiple residues on TMH3/6/7 and the EC-3 loop (see Fig. 5D). Although intramolecular hydrogen bonding and acceptance of hydrogen bonds with water continues to occur, the primary donor of hydrogen bonding to the 2-AG headgroup hydroxyls is D(275) in the EC-3 loop, and S6.58 also acts as a hydrogen bond donor with the headgroup hydroxyls but to a much lesser extent. Overall, in the sequence trajectory C \rightarrow E (up to protonation point) \rightarrow F \rightarrow G, the most commonly seen hydrogen bonds are an intramolecular hydrogen bond between the two hydroxyl groups in 2-AG, hydrogen bonds with water, and frequent interaction with D(275) after 2-AG enters CB2. It is clear in Fig. 5D that a portion of the 2-AG acyl chain remains in lipid. This is true to the end of trajectory G.

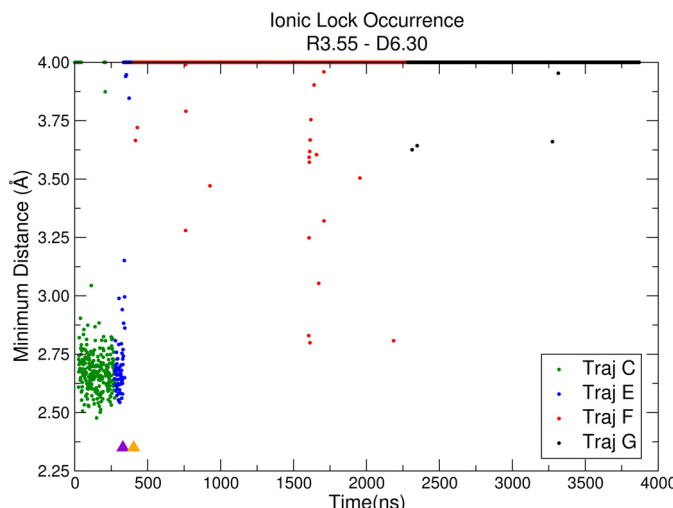


FIGURE 9. This figure provides a plot of the N(R3.55(136))-O(D6.30(240)) distance versus time for the sequence trajectory C → E (up to protonation point) → trajectory F → G. The purple arrowhead marks the point at which CB2 was protonated. The ionic lock salt bridge between R3.55(136) and D6.30(240) was considered broken if the N(R3.55(136))-O(D6.30(240)) distance was 4 Å or greater. Distances greater than or equal to 4 Å were plotted at 4 Å.

Toggle Switch—An important conformational change within the ligand binding pocket that has been documented to occur upon light activation of rhodopsin is a change in the W6.48 χ_1 torsion angle from *g*⁺ to *trans* (22, 56). In the dark (inactive) state of rhodopsin, the β -ionone ring of 11-*cis*-retinal is close to W6.48(265) and acts as a linchpin, constraining W6.48 in a $\chi_1 = g^+$ conformation (12). In the light-activated state, the β -ionone ring moves away from TMH6 and toward TMH4, where it resides close to A4.58(169) (57). This movement releases the constraint on W6.48(265), making it possible for W6.48(265) to undergo a conformational change. Lin and Sakmar (25) reported that perturbations in the environment of W6.48(265) of rhodopsin occur during the conformational change concomitant with receptor activation. This suggests that the conformation of W6.48(265) when rhodopsin is in its inactive/ground state (*R*; $\chi_1 = g^+$) changes during activation (*i.e.* W6.48(265) $\chi_1 g^+ \rightarrow trans$). In many other GPCRs, this change is part of a concerted movement of W6.48 and adjacent residues with this set of residues called the “rotamer toggle switch” (51, 58). Fig. 10 illustrates that I5.47(198)/F3.36(117)/W6.48(258) may constitute the rotamer toggle switch for the CB2 receptor. In Fig. 10A at the start of trajectory G, I5.47(198) has a *g*⁺ χ_1 . This places a methyl group (*dashed circle*) adjacent to W6.48(258) and fills the space needed for a W6.48(258) $\chi_1 g^+ \rightarrow trans$ change. At 912 ns into trajectory G (Fig. 10B), I5.47(198) undergoes a $\chi_1 g^+ \rightarrow g^-$ transition that creates an open space (*circled*) adjacent to W6.48(258). At 913 ns into trajectory G, W6.48(258) undergoes the $\chi_1 g^+ \rightarrow trans$ change, and F3.36(117) undergoes a $\chi_1 trans \rightarrow g^+$ change concomitantly. This change in F3.36(117) effectively prevents the movement of the W6.48(258) back to its original position in the bundle, even when at 988 ns into trajectory G (Fig. 10D) the χ_1 of W6.48(258) returns to *g*⁺ and its χ_2 moves to *trans*.

Water Density—Fig. 11A illustrates the location of water (shown in green) before 2-AG entry from the beginning of tra-

jectory C up to 53 ns in trajectory E. Fig. 11B illustrates the water location (shown in orange) after 2-AG entry and the subsequent W6.48 conformational change (913–1668 ns, trajectory G). Before ligand entry, there is some water in the binding pocket. However, ligand binding and the subsequent W6.48 conformational change results in a continuous channel of water from the extracellular domain through the binding pocket to the intracellular domain of the receptor.

DISCUSSION

Ligand Binding via the Lipid Bilayer—Our results suggest that 2-AG (which contains the polyunsaturated arachidonic acid chain (20:4, *n*-6)) can enter CB2 from the lipid bilayer after partitioning out of bulk lipid at the TMH6/7 interface and encouraging the subsequent formation of an opening between TMH6/7 (Fig. 4, *top* and *bottom*). This association with the TMH6/7 interface appears to be very specific, because although 38 2-AGs were placed in bulk lipid around the CB2 bundle, partitioning occurred only at the TMH6/7 interface. ¹H magic angle spinning NMR experiments have shown that the surface of rhodopsin has sites for specific interaction with lipids (59), and MD simulations have shown that the polyunsaturated fatty acid docosahexaenoic acid (22:6, *n*-3) routinely forms tight associations with rhodopsin in a small number of specific locations. Furthermore, the same calculations showed that the presence of tightly packed docosahexaenoic acid molecules tends to weaken interhelical packing (36).

The orientation of both classical and endogenous cannabinoid ligands in the lipid bilayer has been established by small angle x-ray diffraction/differential calorimetry experiments (60), as well as by NMR (61, 62). These studies have shown that the C-3 side chain of classical cannabinoids is aligned parallel with the membrane acyl chains (60, 62) and that the fatty acid chain of endogenous cannabinoids orients parallel to membrane acyl chains with terminal methyl near the center of the bilayer (61). Cannabinoid ligand entry at the TMH6/7 interface is supported by isothiocyanate labeling studies of CB2 using the classical cannabinoid, AM841 functionalized at the C-3 dimethylheptyl side chain terminal carbon (1). Despite the fact that C7.42(288) faces into the CB2 binding pocket and would be a likely covalent attachment site if the ligand entered the CB2 binding pocket in the traditional way (from extracellular), AM841 was found to selectively label only one Cys residue, C6.47(257) (1). This residue is located in the TMH6/7 interface, facing lipid in our CB2 model. This residue also faces lipid in the rhodopsin (12–15), β_2 -AR (16–18), β_1 -AR (19), and adenosine A2A receptor (20) crystal structures. Furthermore, CB2 receptor substituted cysteine accessibility method studies have indicated that C6.47(257) is not accessible from within the CB2 ligand binding pocket (35). This suggests that AM841 may covalently label the outside-facing C6.47(257) as it is gaining entrance to the binding domain. Interestingly, AM841 has also been shown to selectively label C6.47 in the cannabinoid CB1 receptor, suggesting that a lipid pathway for ligand entry may also exist for the CB1 receptor (63).

Lipid Pathway for CB2 Ligand Binding

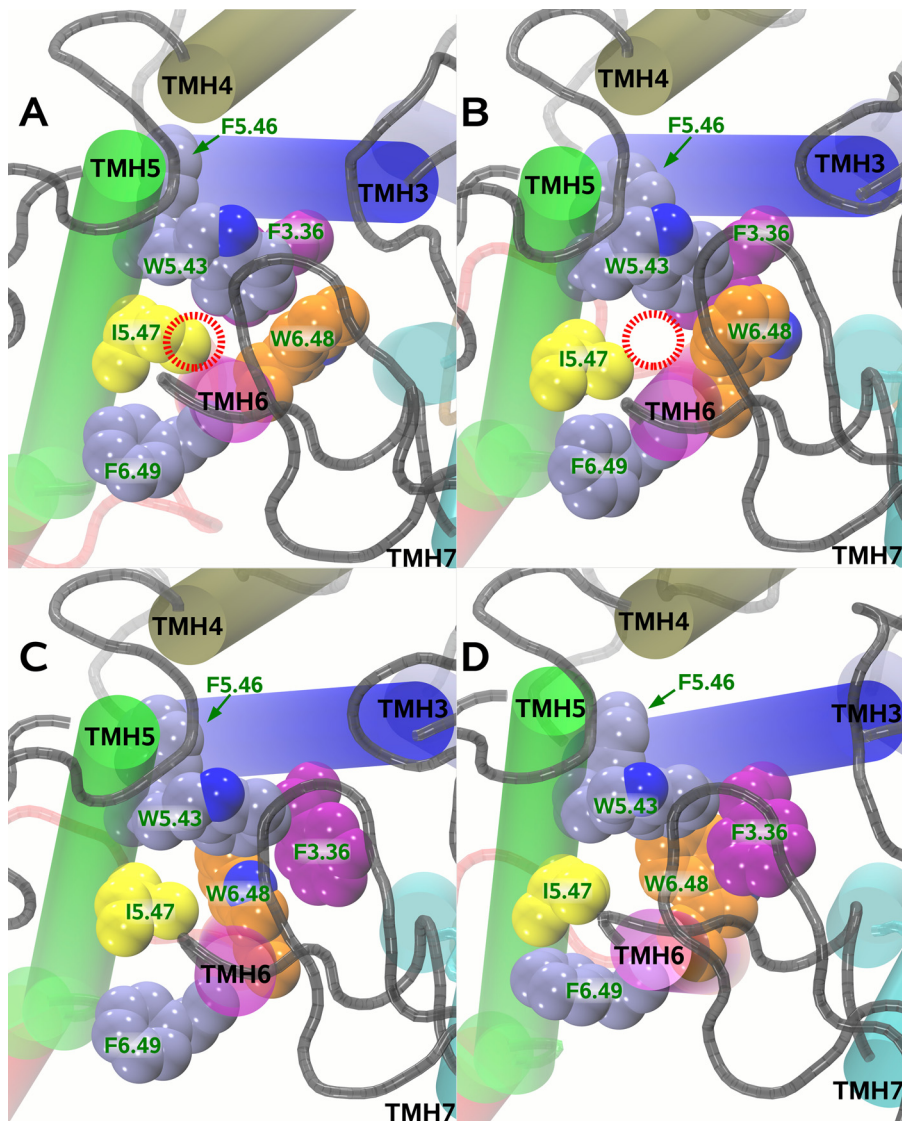


FIGURE 10. This figure illustrates that I5.47(198)/F3.36(117)/W6.48(258) may constitute the toggle switch for the CB2 receptor. *A*, at the start of trajectory G, I5.47(198) has a g^+ χ_1 . This places a methyl group (dashed circle) adjacent to W6.48(258) and fills the space needed for a W6.48(258) χ_1 $g^+ \rightarrow$ $trans$ change. *B*, at 912 ns into trajectory G, I5.47(198) undergoes a χ_1 $g^+ \rightarrow$ g^- transition that creates an open space (dashed circle) adjacent to W6.48(258). *C*, at 913 ns into trajectory G, W6.48(258) undergoes a χ_1 $g^+ \rightarrow$ $trans$ change and F3.36(117) undergoes a χ_1 $trans \rightarrow$ g^+ change concomitantly. This change in F3.36(117) effectively prevents the movement of the W6.48 back to its original position in the bundle, even when *D* at 988 ns into trajectory G, the χ_1 of W6.48(258) returns to g^+ and its χ_2 moves to $trans$.

In the rhodopsin/opsin literature, there is evidence that 11-*cis*-retinal may enter opsin via the lipid bilayer. Park *et al.* (64) identified two openings in the retinal-binding pocket in opsin as follows: an entry site opening between TMH5/6 and an exit site between TMH7/1. Recent computational studies of retinal release and uptake suggest that the TMH5/6 portal may serve both as the uptake and release site (65).

Ionic Lock in CB2—At their intracellular ends, TMH3 and -6 in rhodopsin are constrained by a E3.49(134)/R3.50(135)/E6.30(247) salt bridge that limits the relative mobility of the cytoplasmic ends of TMH3/6 in the inactive state (12) and acts like an ionic lock (66, 67). This ionic lock is not present in other GPCR crystal structures (16–20, 22) possibly because of modifications made to the IC-3 loop to facilitate crystallization. Recent molecular dynamics calculations

suggest that inactive β_2 -AR exists in equilibrium between conformations with the R3.50-D6.30 lock formed and the lock broken, whether or not the co-crystallized ligand is present (68), and MD simulations of the β_1 -AR and β_2 -AR in a lipid bilayer under physiological conditions show that the equilibrated receptors recover this ionic lock (69).

A charge-neutralizing CB2 D6.30(240)N mutation has been reported that resulted in normal ligand binding but a decrease in maximum response of the mutant compared with wild type CB2, suggesting that D6.30(240) is essential for full activation of CB2 (70). Mutations of the CB2 TMH3 DRY motif (71) showed that a Y3.51(132)A mutation had the greatest impact on signal transduction. Our CB2 R simulation results are consistent with both of these mutation studies as they suggest that a reinforced interaction involving both D6.30(240) and Y3.51(132) is important to maintain the inactive state TMH3/6 interaction in CB2.

Changes in Internal Hydration—Recent microsecond time scale MD simulations of rhodopsin have shown a dramatic increase in internal hydration upon activation (30). Along the same lines, simulations of apo- β_2 -AR also showed very high internal hydration, under conditions where the protein is expected to show some degree of activation (72). The degree of core hydration seen after W6.48(258) in CB2 undergoes its conformational

change (Fig. 11B) is comparable with that seen for rhodopsin.

CB2 Activation—Trajectory E shows the first two major occurrences upon ligand entry that are associated with GPCR activation as follows: 1) the D6.30(240)/R3.55(136) salt bridge (along with the Y3.51(132)/L6.29(239) hydrogen bond) breaks (Fig. 3, lower right), and 2) the IC helical extensions of TMH5 and TMH6 (IC-3 loop) then hinge and move away from the TMH bundle and up toward lipid. In trajectory E, however, the simulation does not achieve a full activated state as the putative toggle switch, which involves a W6.48 χ_1 $g^+ \rightarrow$ $trans$ change (22, 51, 58) has not yet occurred. 133 ns after the intracellular end of CB2 opened (with 2-AG entry) in trajectory E, the salt bridge between D6.30(240) and R3.55(136) re-formed and the IC-3 loop hinged back to its original position.

Lipid Pathway for CB2 Ligand Binding

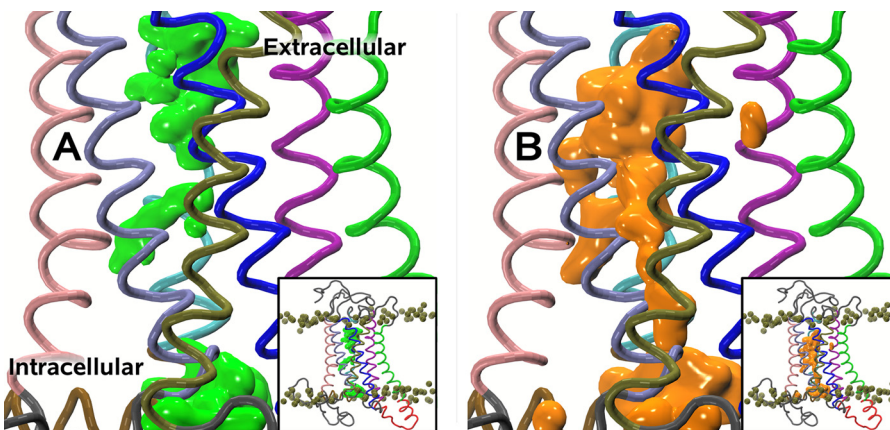


FIGURE 11. *A*, water location (shown in green surface display) before 2-AG entry 53 ns into trajectory *E*. *B*, water location (shown in orange surface display) after 2-AG entry (913–1668 ns, trajectory *G*). Here, the TMHs have been assigned the following colors: TMH1 (pink), TMH2 (gray), TMH3 (dark blue), TMH4 (gold), TMH5 (green), TMH6 (magenta), TMH7 (cyan), and Hx8 (brown). Insets illustrate the position of the phosphorus atoms (colored gold) of the lipid bilayer relative to the TMH bundle in both *A* and *B*.

It seems likely that this salt bridge reformed because the protonation step had not occurred. pH-dependent activation studies in β_2 -AR (29) and flash photolysis experiments on rhodopsin (73, 74) have shown that activation is linked to a rapid uptake of two protons. Those studies indicate that E/D3.49 is likely one of the sites, although the second site has been suggested to be E3.28 (55) for rhodopsin and E/D6.30 for the β_2 -AR (66) and 5HT-2A (67) receptors. A study of the sequence of late molecular events in the activation of rhodopsin suggests that the movement of TMH6 precedes proton uptake from solution and transducin binding (54). Consistent with this result, the conformational changes that occur upon rhodopsin activation have been reported to occur before the protonation of E3.49(134) (31). Thus, it appears that trajectory *E* captured the beginning of ligand-initiated CB2 activation.

To effect the proton uptake, we took the frame at 127 ns into trajectory *E*, a frame at which the CB2 IC domain remained open, and protonated D3.49(130) and D6.30(240). A new (NVT) simulation was begun from this point, trajectory *F*. This trajectory was run for 1.954 μ s. Trajectory *G* (NVE) was begun from the last frame of trajectory *F* and was run for 1.668 μ s. At 913 ns into trajectory *G*, the W6.48 $\chi_1 g+ \rightarrow trans$ change in the ligand binding pocket occurred and was followed by a large influx of water. Thus, over the sequence, trajectory *F* \rightarrow *G*, the simulation achieved the two additional changes associated with GPCR activation as follows: 1) W6.48 toggle switch conformational change and 2) water influx.

It is interesting that the W6.48 toggle switch was triggered at a latter stage in the CB2 simulation. For rhodopsin, this is an early occurrence because it is triggered by the isomerization of 11-cis-retinal inside the ligand binding pocket in response to light. The CB2 receptor requires a diffusing ligand to enter its ligand binding pocket. Because 2-AG approaches CB2 from the bilayer in the simulations reported here and enters CB2 between TMH6 and TMH7, 2-AG is able to cause changes in the TMH3/6 ionic lock before enough of its bulk has entered the binding pocket to effect changes within. Thus, the toggle switch change occurring at a later stage here would be expected.

Time Scale for GPCR Activation—

In the work reported here, ligand-induced CB2 receptor activation was observed on a microsecond time scale. This is a much shorter time scale than the millisecond time scale reported for light activation of rhodopsin (74) or the seconds reported for β_2 -AR activation in living cells (28). It is important to emphasize the following. 1) The simulations reported here were begun with the ligand near the receptor, significantly reducing ligand diffusion times. 2) 2-AG did not enter the receptor in every simulation. 3) The protonation changes, which are likely to be a rate-limiting step in activation, were applied manually.

- 4) What is observed here are conformational changes known to occur during GPCR activation; however, the G protein coupling step is not simulated here.

Acknowledgments—We acknowledge the contributions of the Blue Matter team (B. Fitch, R. Germain, A. Rayshubskiy, T. J. C. Ward, M. Eleftheriou, F. Suits, Y. Zhestkov, R. Zhou, J. Pitera, and W. Swope) and IBM Watson Research for use of the BGW Blue Gene facility.

REFERENCES

1. Pei, Y., Mercier, R. W., Anday, J. K., Thakur, G. A., Zvonok, A. M., Hurst, D., Reggio, P. H., Janero, D. R., and Makriyannis, A. (2008) *Chem. Biol.* **15**, 1207–1219
2. Munro, S., Thomas, K. L., and Abu-Shaar, M. (1993) *Nature* **365**, 61–65
3. Galiègue, S., Mary, S., Marchand, J., Dussossoy, D., Carrière, D., Carayon, P., Bouaboula, M., Shire, D., Le Fur, G., and Casellas, P. (1995) *Eur. J. Biochem.* **232**, 54–61
4. Howlett, A. C., Barth, F., Bonner, T. I., Cabral, G., Casellas, P., Devane, W. A., Felder, C. C., Herkenham, M., Mackie, K., Martin, B. R., Mechoulam, R., and Pertwee, R. G. (2002) *Pharmacol. Rev.* **54**, 161–202
5. Benito, C., Núñez, E., Tolón, R. M., Carrier, E. J., Rábano, A., Hillard, C. J., and Romero, J. (2003) *J. Neurosci.* **23**, 11136–11141
6. Van Sickle, M. D., Duncan, M., Kingsley, P. J., Mouihate, A., Urbani, P., Mackie, K., Stella, N., Makriyannis, A., Piomelli, D., Davison, J. S., Marnett, L. J., Di Marzo, V., Pittman, Q. J., Patel, K. D., and Sharkey, K. A. (2005) *Science* **310**, 329–332
7. Mechoulam, R., Ben-Shabat, S., Hanus, L., Ligumsky, M., Kaminski, N. E., Schatz, A. R., Gopher, A., Almog, S., Martin, B. R., and Compton, D. R. (1995) *Biochem. Pharmacol.* **50**, 83–90
8. Sugiyama, T., Kondo, S., Sukagawa, A., Nakane, S., Shinoda, A., Itoh, K., Yamashita, A., and Waku, K. (1995) *Biochem. Biophys. Res. Commun.* **215**, 89–97
9. Piomelli, D. (2003) *Nat. Rev. Neurosci.* **4**, 873–884
10. Di Marzo, V. (2008) *Nat. Rev. Drug Discov.* **7**, 438–455
11. Dinh, T. P., Carpenter, D., Leslie, F. M., Freund, T. F., Katona, I., Sensi, S. L., Kathuria, S., and Piomelli, D. (2002) *Proc. Natl. Acad. Sci. U.S.A.* **99**, 10819–10824
12. Palczewski, K., Kumada, T., Hori, T., Behnke, C. A., Motohashima, H., Fox, B. A., Le Trong, I., Teller, D. C., Okada, T., Stenkamp, R. E., Yamamoto, M., and Miyano, M. (2000) *Science* **289**, 739–745
13. Li, J., Edwards, P. C., Burghammer, M., Villa, C., and Schertler, G. F. (2004) *J. Mol. Biol.* **343**, 1409–1438
14. Okada, T., Fujiyoshi, Y., Silow, M., Navarro, J., Landau, E. M., and

Lipid Pathway for CB2 Ligand Binding

- Shichida, Y. (2002) *Proc. Natl. Acad. Sci. U.S.A.* **99**, 5982–5987
15. Okada, T., Sugihara, M., Bondar, A. N., Elstner, M., Entel, P., and Buss, V. (2004) *J. Mol. Biol.* **342**, 571–583
16. Rosenbaum, D. M., Cherezov, V., Hanson, M. A., Rasmussen, S. G., Thian, F. S., Kobilka, T. S., Choi, H. J., Yao, X. J., Weis, W. I., Stevens, R. C., and Kobilka, B. K. (2007) *Science* **318**, 1266–1273
17. Cherezov, V., Rosenbaum, D. M., Hanson, M. A., Rasmussen, S. G., Thian, F. S., Kobilka, T. S., Choi, H. J., Kuhn, P., Weis, W. I., Kobilka, B. K., and Stevens, R. C. (2007) *Science* **318**, 1258–1265
18. Rasmussen, S. G., Choi, H. J., Rosenbaum, D. M., Kobilka, T. S., Thian, F. S., Edwards, P. C., Burghammer, M., Ratnala, V. R., Sanishvili, R., Fischetti, R. F., Schertler, G. F., Weis, W. I., and Kobilka, B. K. (2007) *Nature* **450**, 383–387
19. Warne, T., Serrano-Vega, M. J., Baker, J. G., Moukhametzianov, R., Edwards, P. C., Henderson, R., Leslie, A. G., Tate, C. G., and Schertler, G. F. (2008) *Nature* **454**, 486–491
20. Jaakola, V. P., Griffith, M. T., Hanson, M. A., Cherezov, V., Chien, E. Y., Lane, J. R., Ijzerman, A. P., and Stevens, R. C. (2008) *Science* **322**, 1211–1217
21. Wess, J. (1997) *FASEB J.* **11**, 346–354
22. Kobilka, B. K., and Deupi, X. (2007) *Trends Pharmacol. Sci.* **28**, 397–406
23. Farrens, D. L., Altenbach, C., Yang, K., Hubbell, W. L., and Khorana, H. G. (1996) *Science* **274**, 768–770
24. Ghanouni, P., Steenhuis, J. J., Farrens, D. L., and Kobilka, B. K. (2001) *Proc. Natl. Acad. Sci. U.S.A.* **98**, 5997–6002
25. Lin, S. W., and Sakmar, T. P. (1996) *Biochemistry* **35**, 11149–11159
26. Javitch, J. A., Fu, D., Liapakis, G., and Chen, J. (1997) *J. Biol. Chem.* **272**, 18546–18549
27. Jensen, A. D., Guarnieri, F., Rasmussen, S. G., Asmar, F., Ballesteros, J. A., and Gether, U. (2001) *J. Biol. Chem.* **276**, 9279–9290
28. Nakanishi, J., Takarada, T., Yunoki, S., Kikuchi, Y., and Maeda, M. (2006) *Biochem. Biophys. Res. Commun.* **343**, 1191–1196
29. Ghanouni, P., Schambye, H., Seifert, R., Lee, T. W., Rasmussen, S. G., Gether, U., and Kobilka, B. K. (2000) *J. Biol. Chem.* **275**, 3121–3127
30. Grossfield, A., Pitman, M. C., Feller, S. E., Soubias, O., and Gawrisch, K. (2008) *J. Mol. Biol.* **381**, 478–486
31. Mahalingam, M., Martínez-Mayorga, K., Brown, M. F., and Vogel, R. (2008) *Proc. Natl. Acad. Sci. U.S.A.* **105**, 17795–17800
32. Ballesteros, J. A., and Weinstein, H. (1995) in *Methods in Neuroscience* (Sealfon, S. C., ed) pp. 366–428, Academic Press, San Diego
33. Nebane, N. M., Hurst, D. P., Carrasquer, C. A., Qiao, Z., Reggio, P. H., and Song, Z. H. (2008) *Biochemistry* **47**, 13811–13821
34. Song, Z. H., Slowey, C. A., Hurst, D. P., and Reggio, P. H. (1999) *Mol. Pharmacol.* **56**, 834–840
35. Zhang, R., Hurst, D. P., Barnett-Norris, J., Reggio, P. H., and Song, Z. H. (2005) *Mol. Pharmacol.* **68**, 69–83
36. Grossfield, A., Feller, S. E., and Pitman, M. C. (2006) *Proc. Natl. Acad. Sci. U.S.A.* **103**, 4888–4893
37. MacKerell, A. D., Jr., Bashford, D., Bellott, M., R. L. Dunbrack, R. L., Jr., Evanseck, J. D., Field, M. J., Fischer, S., Gao, J., Guo, H., Ha, S., Joseph-McCarthy, D., Kuchnir, L., Kuczera, K., Lau, F. T. K., Mattos, C., Michnick, S., Ngo, T., Nguyen, D. T., Prodhom, B., Reiher, W. E., III, Roux, B., Schlenkrich, M., Smith, J. C., Stote, R., Straub, J., Watanabe, M., Wiorkiewicz-Kuczera, J., Yin, D., and Karplus, M. (1998) *J. Phys. Chem. B* **102**, 3586–3616
38. Feller, S. E., and MacKerell, A. D., Jr. (2000) *J. Phys. Chem. B* **104**, 7510–7515
39. Pitman, M. C., Suits, F., MacKerell, A. D., Jr., and Feller, S. E. (2004) *Biochemistry* **43**, 15318–15328
40. Swope, W. C., Andersen, H., Berens, P. H., and Wilson, K. R. (1982) *J. Chem. Phys.* **76**, 637–649
41. Andersen, H. (1983) *J. Comput. Phys.* **52**, 24–34
42. Gara, A., Blumrich, M. A., Chen, D., Chiu, G. L., Coteus, P., Giampapa, M. E., Haring, R. A., Heidelberger, P., Hoenicke, D., Kopcsay, G. V., Liebsch, T. A., Ohmacht, M., Steinmacher-Burow, B. D., Takken, T., and Vranas, P. (2005) *IBM J. Res. Dev.* **49**, 195–212
43. Fitch, B. G., Rayshubskiy, A., Eleftheriou, M., Ward, T. J., Giampapa, M., Zhestkov, Y., Pitman, M. C., Suits, F., Grossfield, A., Pitera, J., Swope, W. C., Zhou, R., Feller, S. E., and Germain, R. S. (2006) in *International Conference on Computational Science* (Alexandrov, V., Albada, D. V., Sloot, P., and Dongarra, J., eds) pp. 846–854, Springer-Verlag, New York
44. Fitch, B. G., Germain, R. S., Mendell, M., Pitera, J., Pitman, M. C., Rayshubskiy, A., Sham, Y., Suits, F., Swope, W. C., Ward, T. J., Zhestkov, Y., and Zhou, R. (2003) *J. Para. Distrib. Comp.* **63**, 759–773
45. Lau, P. W., Grossfield, A., Feller, S. E., Pitman, M. C., and Brown, M. F. (2007) *J. Mol. Biol.* **372**, 906–917
46. Martínez-Mayorga, K., Pitman, M. C., Grossfield, A., Feller, S. E., and Brown, M. F. (2006) *J. Am. Chem. Soc.* **128**, 16502–16503
47. Pitman, M. C., Grossfield, A., Suits, F., and Feller, S. E. (2005) *J. Am. Chem. Soc.* **127**, 4576–4577
48. Musafia, B., Buchner, V., and Arad, D. (1995) *J. Mol. Biol.* **254**, 761–770
49. Humphrey, W., Dalke, A., and Schulter, K. (1996) *J. Mol. Graph.* **14**, 33–38
50. Romo, T. D., and Grossfield, A. (2009) *31st Annual International Conference of the IEEE EMBS, Minneapolis, MN*, pp. 2332–2335, Springer-Verlag, New York
51. McAllister, S. D., Hurst, D. P., Barnett-Norris, J., Lynch, D., Reggio, P. H., and Abood, M. E. (2004) *J. Biol. Chem.* **279**, 48024–48037
52. Scheerer, P., Park, J. H., Hildebrand, P. W., Kim, Y. J., Krauss, N., Choe, H. W., Hofmann, K. P., and Ernst, O. P. (2008) *Nature* **455**, 497–502
53. Ballesteros, J., Kitanovic, S., Guarnieri, F., Davies, P., Fromme, B. J., Konvicka, K., Chi, L., Millar, R. P., Davidson, J. S., Weinstein, H., and Sealfon, S. C. (1998) *J. Biol. Chem.* **273**, 10445–10453
54. Knierim, B., Hofmann, K. P., Ernst, O. P., and Hubbell, W. L. (2007) *Proc. Natl. Acad. Sci. U.S.A.* **104**, 20290–20295
55. Fahmy, K., Jäger, F., Beck, M., Zvyaga, T. A., Sakmar, T. P., and Siebert, F. (1993) *Proc. Natl. Acad. Sci. U.S.A.* **90**, 10206–10210
56. Reggio, P. H. (2006) *AAPS J.* **8**, E322–E336
57. Borhan, B., Souto, M. L., Imai, H., Shichida, Y., and Nakanishi, K. (2000) *Science* **288**, 2209–2212
58. Shi, L., Liapakis, G., Xu, R., Guarnieri, F., Ballesteros, J. A., and Javitch, J. A. (2002) *J. Biol. Chem.* **277**, 40989–40996
59. Soubias, O., Teague, W. E., and Gawrisch, K. (2006) *J. Biol. Chem.* **281**, 33233–33241
60. Mavromoustakos, T., Yang, D. P., Broderick, W., Fournier, D., and Makriyannis, A. (1991) *Pharmacol. Biochem. Behav.* **40**, 547–552
61. Tian, X., Guo, J., Yao, F., Yang, D. P., and Makriyannis, A. (2005) *J. Biol. Chem.* **280**, 29788–29795
62. Kimura, T., Cheng, K., Rice, K. C., and Gawrisch, K. (2009) *Biophys. J.* **96**, 4916–4924
63. Picone, R. P., Khanolkar, A. D., Xu, W., Ayotte, L. A., Thakur, G. A., Hurst, D. P., Abood, M. E., Reggio, P. H., Fournier, D. J., and Makriyannis, A. (2005) *Mol. Pharmacol.* **68**, 1623–1635
64. Park, J. H., Scheerer, P., Hofmann, K. P., Choe, H. W., and Ernst, O. P. (2008) *Nature* **454**, 183–187
65. Hildebrand, P. W., Scheerer, P., Park, J. H., Choe, H. W., Piechnick, R., Ernst, O. P., Hofmann, K. P., and Heck, M. (2009) *PLoS ONE* **4**, e4382
66. Ballesteros, J. A., Jensen, A. D., Liapakis, G., Rasmussen, S. G., Shi, L., Gether, U., and Javitch, J. A. (2001) *J. Biol. Chem.* **276**, 29171–29177
67. Visiers, I., Ebersole, B. J., Dracheva, S., Ballesteros, J., Sealfon, S. C., and Weinstein, H. (2002) *Int. J. Quantum Chem.* **88**, 65–75
68. Dror, R. O., Arlow, D. H., Borhani, D. W., Jensen, M. Ø., Piana, S., and Shaw, D. E. (2009) *Proc. Natl. Acad. Sci. U.S.A.* **106**, 4689–4694
69. Vanni, S., Neri, M., Tavernelli, I., and Rothlisberger, U. (2009) *Biochemistry* **48**, 4789–4797
70. Nebane, N. M., Kellie, B., and Song, Z. H. (2006) *FEBS Lett.* **580**, 5392–5398
71. Rhee, M. H., Nevo, I., Levy, R., and Vogel, Z. (2000) *FEBS Lett.* **466**, 300–304
72. Romo, T. R., Grossfield, A., and Pitman, M. C. (2010) *Biophys. J.* **98**, 76–84
73. Arnis, S., and Hofmann, K. P. (1993) *Proc. Natl. Acad. Sci. U.S.A.* **90**, 7849–7853
74. Arnis, S., Fahmy, K., Hofmann, K. P., and Sakmar, T. P. (1994) *J. Biol. Chem.* **269**, 23879–23881